Solid State Communications 252 (2017) 16–21

Contents lists available at ScienceDirect

Solid State Communications

journal homepage: www.elsevier.com/locate/ssc

Communication

The coupled effects of oxygen defect and crystallographic orientation on the electromechanical properties of $BaTiO_3$ nanowires

Saeed Ghorbanali[a,*], Mehran Gholipour Shahraki[b]

[a] Department of Physics, Tafresh University, Tafresh 39518-79611, Iran
[b] Physics Department, Faculty of Science, Arak University, Arak 38156-8-8349, Iran

ARTICLE INFO

Keywords:
Oxygen vacancy
$BaTiO_3$ Nanowires
Piezoelectric
Electromechanical properties
Core-shell model

ABSTRACT

Influence of oxygen vacancies on electromechanical properties of individual $BaTiO_3$ (BTO) nanowires (NWs) is investigated, using molecular dynamics simulations. The simulations were performed for defected 0–4% oxygen vacancy defects) tetragonal NWs with axial directions of [001] and [110]. Results show an increase in spontaneous polarization and piezoelectric constant of the individual NWs due to increasing oxygen vacancy concentration, and a decrease in yield stress and Young's modulus. It seems that in individual BTO NWs the softening effect of the oxygen vacancies overcomes the pinning effect and results in enhancement of piezoelectric constant and spontaneous polarization. Results also show that yield stress and Young's modulus of the NWs with axial direction of [001] are higher than those for NWs with axial direction of [110] while it is reverse for spontaneous polarization and piezoelectric constant.

1. Introduction

Piezoelectric nanogenerators (NGs) are highly sought for harvesting ambient mechanical energy and powering small electronic devices [1–4]. These NGs have the ability to scavenge energy directly from ambient mechanical sources such as wind, waves and noise [5–7] to power wireless electronic devices. They also can convert biomechanical energies such as, muscle energy, heart beats or even blood flow [8–11] into electricity to run implantable biodevices and biomedical sensors. Among the piezoelectric nanostructures, BTO nanostructures are highly investigated due to their excellent piezoelectric and dielectric properties and also their environmentally safe nature. Because of these advantages, a great deal of experimental and theoretical research has focused on synthesis, investigation and application of these nanostructures. Zhang et al. fabricated a supper flexible NG based on BTO nanowires [12]. The nanogenerator was fixed on a human finger and produced an output voltage up to 0.9 V and an output current up to 10.5 nA, when the finger was bent. A flexible high performance NG based on composite thin films was fabricated by Shin and coworkers which could produce an output voltage of 75 V at the applied force normal to the surface [13]. Jeong et al. [14] synthesized BTO nanocrystals on biotempelate of M13 to fabricate a high-performance flexible nanogenerator. Koka et al. designed a vertically aligned BTO nanowires array with a power density 16 times greater than a similar ZnO based system [15]. Because of excellent electrical properties of BTO, many attempts are made to enhance the piezoelectric property of BTO nanostructures to improve efficiency of NGs. It is shown that doping of BTO ceramics by aluminum atoms can enhance its piezoelectric property [16]. Devi et al. substituted Tungsten with Ti to synthesize $BaTi_{(1-x)}W_{(x)}O_3$, using a solid-state reaction method. In their work, formation of a single-phase perovskite structure was confirmed by X-ray analysis. They reported an enhancement in polarization by increasing the concentration of Tungsten atoms [17]. Enhancement of piezoelectric constant was also predicted theoretically in domain engineered $(PbTiO_3)(m)/(BaTiO_3)(n)$ ferroelectric superlattices, using a phase field model [18].

Defect engineering is one of the most important techniques used in solid state physics to make desirable changes in physical properties of materials. Oxygen vacancy defects are popular in perovskites and significantly affect physical properties, such as electric and ionic conductivity, as well as magnetic, catalytic, dielectric and ferroelectric properties of perovskites [19–29].

In our previous work, the influence of crystallographic orientation and diameter on electromechanical properties of BTO nanobelts was investigated [30]. In present work, the influence of oxygen vacancy defects on piezoelectric constant, spontaneous polarization, Young's modulus, Yield stress, and mean square distance (MSD) of BTO nanowires will be investigated. Molecular dynamics methods have been employed to examine oxygen defects in tetragonal BTO NWs for [001] and [110] crystallographic orientations over a specific range 0–4%) of oxygen defect.

* Corresponding author.
E-mail addresses: s.ghorbanali@tafreshu.ac.ir (S. Ghorbanali), m-gholipour@araku.ac.ir (M.G. Shahraki).

http://dx.doi.org/10.1016/j.ssc.2017.01.004
Received 10 April 2016; Received in revised form 14 December 2016; Accepted 7 January 2017
Available online 09 January 2017
0038-1098/

2. Simulation method

Molecular dynamics (MD) method is one of the most important simulation techniques in condense matter physics and associated field of nanostructures modeling. Many of the physical parameters such as Young's modulus, yield stress, piezoelectric constant, diffusion coefficient, and ionic conductivity can be evaluated through this method. In this method, the Newton's equation of motion of the N atoms of the system has to be solved [31,32]:

$$\vec{F}_i = \sum_{j\neq i}^{N} \vec{f}\,(\vec{r}_{ij}) = m_i\vec{a}_i = m_i\frac{d^2\vec{r}_i}{dt^2} \tag{1}$$

where, $\vec{a}_i$, m_i,$\vec{r}_i$ are the acceleration, mass and position of the atom i, respectively and $\vec{r}_{ij}$*is* the distance between atoms i and j. The total force acting on the atom i can be evaluated from the gradient of the total potential energy of the system,

$$\vec{F}_i = -\vec{\nabla}_i U_{ij}^{total}.$$

The choice of the potential function is an important option which determinates the accuracy of the calculations in MD simulation. In the study, the shell-model potential was employed to simulate BTO NWs. In the shell -model, each atom is represented by two charged particles: a massive ion-core and a massless ion-shell. The core and shell are connected by a harmonic spring with the potential of $V(\omega) = \frac{1}{2}\,k_2\omega^2$, where ω is the relative core-shell distance. For O ions, a fourth order core shell interaction potential $V(\omega) = \frac{1}{2}\,k_2\omega^2 + \frac{1}{24}\,k_4\omega^4$ along the O^{-2}-Ti^{+4} bond is also considered [33,34]. There are Coulombic interactions between the cores and shells of different atoms, and short-range interactions between shells. The Buckingham potential is used for the Ba–O, Ti–O, and O–O short-range interactions. The short-range Buckingham potential and long-rang interaction Coulombic potential are as follows [35]:

$$U_{ij}^{total} = U_{ij}^{\text{Buckingham}} + U_{ij}^{coulomb} = \sum_{i=1}^{N}\sum_{j\neq i}\left\{A_{ij}\exp\left(\frac{r_{ij}}{\rho}\right) - \left(\frac{B_{ij}}{r_{ij}^6}\right) + \frac{q_i q_j}{4\pi\varepsilon_0 r_{ij}}\right\}, \tag{2}$$

where, the potential parameters [36,37] are presented in Table 1. The potential used in our simulation was developed and widely used for simulation of defected $BaTiO_3$ structures. The potential parameters were evaluated by fitting a proposed functional form to available experimental data such as vacancy formation energies. Recently, Zulueta et al. [38] employed this potential to investigate the influence of oxygen and titanium vacancies on conducting and transport properties of $BaTiO_3$, using molecular dynamics simulations. They reported an enhancement in ionic conductivity of defected $BaTiO_3$ structures.

As mentioned before, the main goal of the study is to investigate the influence of oxygen vacancy defect on electromechanical properties of BTO NWs. Existence of oxygen vacancies in the BTO structure causes the ions' charges deviate from their natural values. Obviously, deviation for each ion is related to its neighboring atoms. Although these deviations can be calculated through advanced quantum computational methods, it is very difficult (or even impossible) to consider these deviations in classical MD. In this work, simply the additional positive charge (which resulted from oxygen vacancies) was divided to the total number of cations (ions with a net positive charge) and the achieved value was subtracted from the charge of each cation to guarantee charge neutrality condition.

In MD simulation, Young's modulus, yield stress, and piezoelectric constant can be evaluated, using a loading procedure, which in this work has been carried out in z-direction.

In this atomistic simulation, stress $\sigma_i^{\alpha\beta}$ under loading of the NWs, was evaluated by [39]:

$$\sigma_i^{\alpha\beta} = \frac{1}{\Omega}\left[-\frac{1}{2}\sum_{i=1}^{N(x)}\sum_{j\neq i}^{N(x)}\frac{\partial E(r_{ij})}{\partial r_{ij}}\frac{r_{ij}^{\alpha}r_{ij}^{\beta}}{r_{ij}} + \sum_{i=1}^{N(x)} m_i v_i^{\alpha} v_i^{\beta}\right], \tag{3}$$

where, E is the total energy of the system of atoms, α and β are the spatial coordinates, $N(x)$ is the total number of particles in the cell located at position x, Ω is the volume occupied by the atoms and m_i is the mass of atom i.

Mean square displacement (MSD) of ions can be obtained at each time of t as [40]:

$$MSD_i(t) = \frac{1}{N_i}\sum_{n=1}^{N_i}\langle r_n(t+dt) - r_n(t)\rangle^2, \tag{4}$$

where, N_i represents the total number of particles and r_n is the position of the geometric center of an ion at certain time of t. For this simulation, oxygen defects were created by random deletion of oxygen atoms from perfect structure of BTO NWs. Each vacancy point has four first neighbors of Ba ions, two Ti ions and eight O ions around itself, as shown in Fig. 1(a). The polarization of the NWs can be evaluated in a single crystallographic unit cell. The origin of polarization is the net displacement of cations with respect to the oxygen octahedral along [001] and [110] orientations [34]. The component of the polarization in the z-direction for defective unit cell is defined by [30]:

$$P_z = \sum_{j=1}^{N}\frac{P_{unit-cell}}{N};\ P_{\text{unit}} = \sum_{i=1}^{M}\frac{z_i q_i}{V_{\text{unit}}}. \tag{5}$$

where z_i and q_i are the z component of position and the electric charge of the ion i, respectively. In each defected BTO NW, the first summation in Eq. (5) is performed on all of the crystallographic unit cells (N) which make the NW, and the second summation is performed on total atoms (M) that make each unit cell. According to the definition, the piezoelectric coefficient can be calculated from the derivative of the polarization with respect to strain for z direction:

$$d_{33}^{eff} = \frac{dP_z}{d\varepsilon_z}, \tag{6}$$

The classical MD simulation was performed by LAMMPS [41], which was adjusted to calculate Buckingham potential using the Wolf summation. The defective NWs were produced by replicating the unit cell in the X and Y and Z-direction, where for NWs with axial direction of [001] the X, Y and Z axes represent [100], [010] and [001] crystallographic orientations, respectively. The BTO NWs have some random oxygen vacancies which were created by random deletion of oxygen atoms from perfect structure with certain distance from each other. Two groups ([001] and [110] crystallographic directions) of BTO NWs with oxygen vacancies of 0%, 1%, 2%, 3%, and 4% and a fixed length of 149.11 Å and a fixed diameter of 28.49 Å were considered for performing this simulation. The number of atoms in each BTO NW is presented in Table 2.

For axial loading in the Z-direction, first the NWs were relaxed using Isobaric-Isothermal (NPT) ensemble at temperature of 373 K to ensure zero pressure of the nanostructures, and then a uniaxial tension

Table 1
Parameters of shell model and Buckingham potential for $BaTiO_3$ NWs.

Atom	Core charge	Shell charge	k_2 (eVÅ^{-2})	K_4 (eVÅ^{-4})
Ba	5.62	−3.76	251.8	–
Ti	*[1]	−1.58	322.0	–
O	0.91	−2.59	31.0(||) 101.27(⊥)	3000.0 (||)
Interaction	A (eV)	ρ (Å)	B_{ij}(eV.Å^6)	R_{cut}^2(Å)
Ba^{+2} - O^{-2}	1214.4	0.3522	8.0	12.0
Ti^{+4} - O^{-2}	877.2	0.3809	9.0	12.0
O^{-2} - O^{-2}	22,764.0	0.1490	43.0	12.0

1) The symbol * means that Ba core charge is obtained with the neutrality condition. The symbol || and ⊥ indicate the directions parallel and perpendicular to the O–Ti bond, respectively.
2) R_{cut} is the cut-off radius.

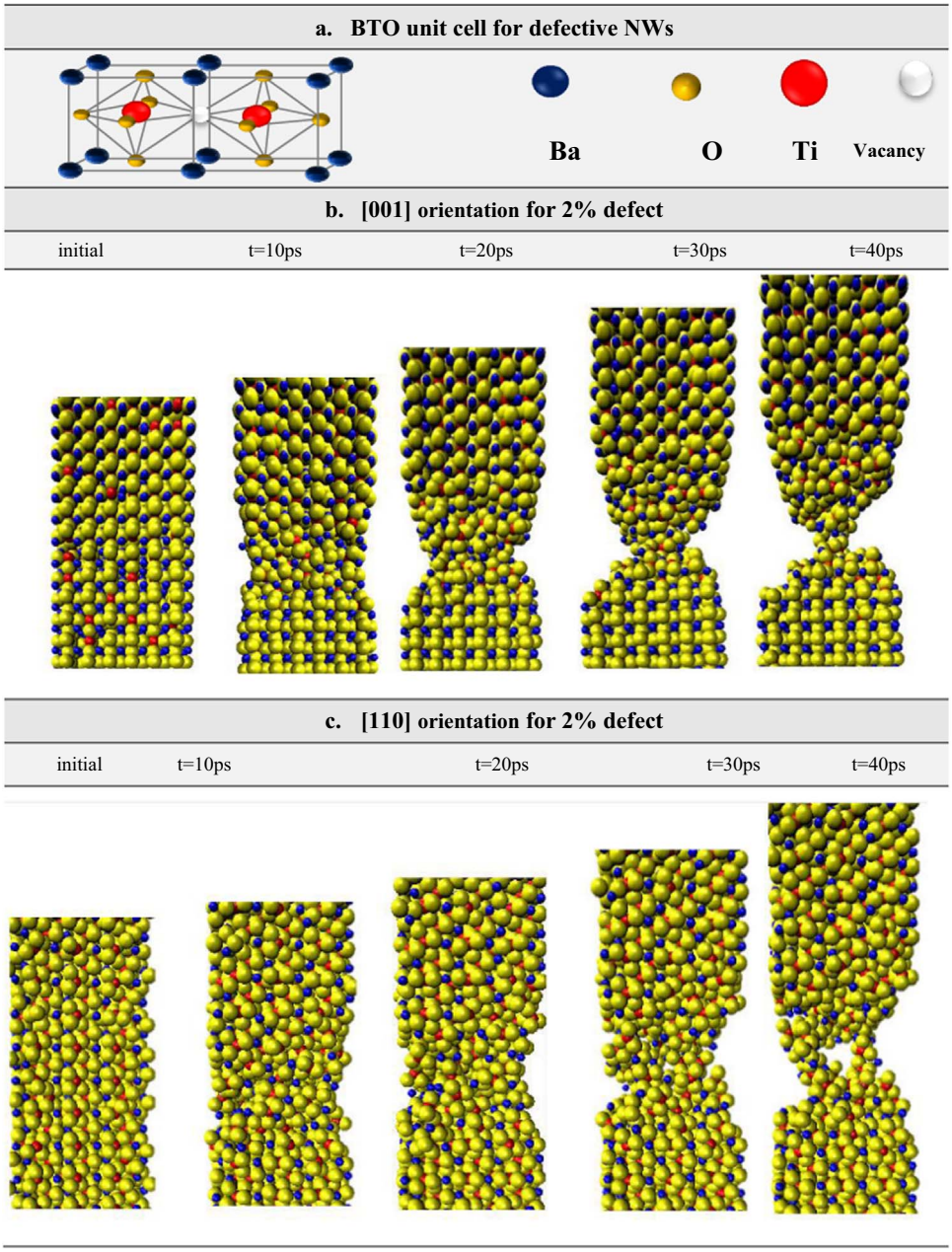

Fig. 1. The perovskite-structured single crystals of BTO, (b,c) Snapshots of the atomic configurations BTO NWs for the [001] and [110] orientations during the tensile stretching process at a substrate temperature of 300 K under different simulation times: the initial equilibrated stage, 10 ps, 20 ps, 30 ps, and 40 ps.

was carried out. The tension was performed by separating the upper and lower layers of atoms as two stiff groups with a rate of 0.01 Å/s. Snapshots of the [001] and [110] nanowires with 2% oxygen vacancy under tensile loading are presented in Figs. (1,b) and (1,c), respectively. Results show that necking has occurred approximately at t=30 ps for both directions and then the necks have deformed to atomic chains at time of 40 ps. The procedure of tension/relaxation continued until the NWs failed. Only with further stretching, a number

Table 2
Number of oxygen (No), titanium (N_{Ti}) and barium (N_{Ba}) atoms in simulated $BaTiO_3$ nanowires. Diameter (D) and length (L) of NWs are specified.

Vacancy concentration	Number of oxygen (N_O)		Number of oxygen (N_O)	
	[001] direction		[110] direction	
Perfect	3996		3972	
1%	3956		3932	
2%	3916		3892	
3%	3876		3852	
4%	3836		3812	
	N_{Ti}=1332	N_{Ba}=1332	N_{Ti}=1324	N_{Ba}=1324
	L=149.11A°	D=33.60A°	L=148.1813A°	D=33.9175A°

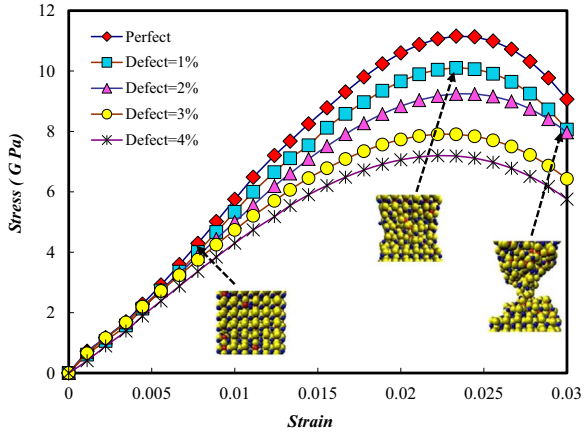

Fig. 2. Stress–strain curves of the BTO NWs with different fractions of random vacancies at 373 K for [001] direction.

of Ba–O and Ti–O bonds are broken at the central section. The equations of motion were integrated via the velocity Verlet algorithm [42]. In order to maintain the NWs temperature, with time steps of 1 fs, the below correction was used [43]:

$$T_D = \frac{u_i^2}{v_i^2} T_A , \tag{7}$$

where, u_i and v_i are the velocity of the ith atom after and before correction and T_D and T_A are the desired and actual temperatures, respectively.

3. Results and discussions

The stress-strain curves for NWs with axial directions of [001] and [110] and various percentage of oxygen vacancies are illustrated in Figs. 2 and 3 and no plastic deformation is observed during this loading procedure. Young's modulus (YG) was calculated from the slope of the stress–strain curve in elastic region [44] and the yield stress was evaluated from the maximum values of the stress-strain curves and the results are depicted in Fig. 4. Given the figures, it can be deduced that the stress will increase by increasing the strain and the YG (slope in the elastic region) and yield stress (YS) both will decrease by vacancy enhancement.

Decreasing YG and YS with oxygen vacancy was also reported in other chemical compounds containing oxygen vacancy, such as cerium oxide [45], yttria stabilized zirconia [46]. Recently, the influence of oxygen vacancy on YG of bulk ZnO has been investigated by Soumya

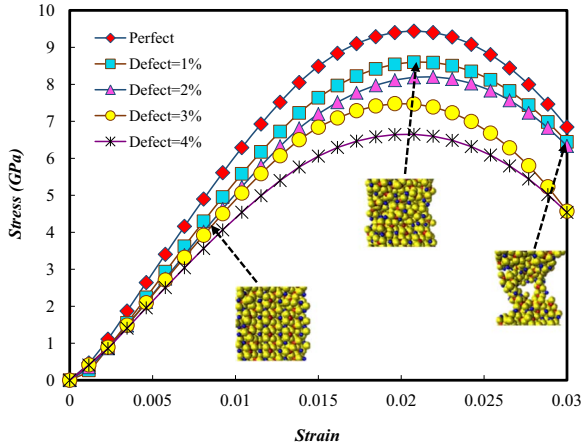

Fig. 3. Stress-strain curves of the BTO NWs with different fractions of vacancies at 373 K for [110] direction.

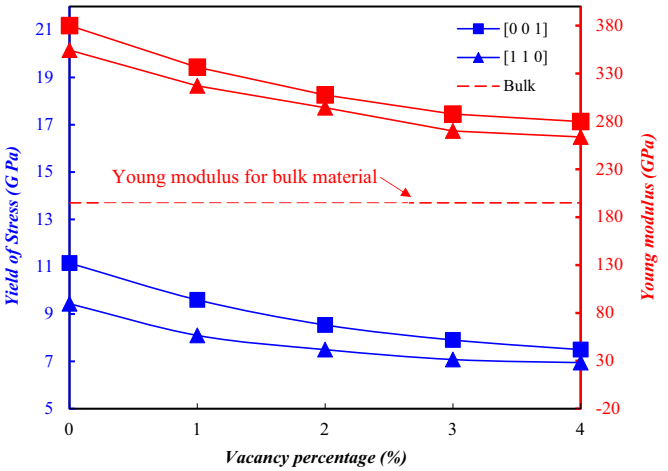

Fig. 4. Variations of Yield of stress and average dislocation in Z direction with vacancy percentage.

et al. [47] using first-principles method. Their results show a reduction in elastic constant of ZnO due to oxygen vacancies which is in agreement with experimental results. Fig. 4 demonstrates that the Young's modulus are higher than that of bulk $BaTiO_3$ [48,49] and obviously reduce with the increase of vacancy percentage.

Effect of oxygen vacancies on mechanical properties of individual ZnO nanowires was experimentally investigated by Lucas et al. [50], using modulated nanoindentation method and an order of magnitude decrease was reported in the elastic modulus of the individual ZnO nanowires.

The mechanism of softening in $BaTiO_3$ has been interpreted by Nowick et al. [51]. In BTO structure, each oxygen vacancy point produces a tetragonal elastic dipole. Moving point defects toward the next sites changes the orientation of these dipoles. The stress-induced ordering of elastic dipole orientations acts as a softening mechanism [51].

Mean square displacement (MSD) of the NWs was evaluated and the results for [001] and [110] orientations are illustrated in Figs. 5 and 6, respectively. Results show an increase in atoms mobility as oxygen vacancy percentage increases. In other words, the stability of the NWs decrease due to increase in vacancy percentage.

If we compare the results for [110] and the [001] orientations, it can be deduced that this effect is more pronounced for the [110] orientation. This phenomenon can be due to the lower ratio of oxygen atoms in this orientation. For a better interpretation of these phenomena, the ratio of N_{Ti}/N_O (number of Ti atoms to number of O atoms) and dislocations of oxygen atoms along the z direction are shown in

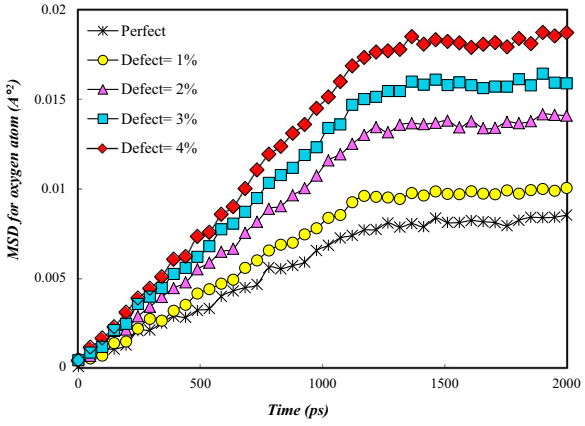

Fig. 5. Oxygen ions mean square displacements versus time in BTO NWs for [110] direction when the vacancy percentage is changed from 0% to 4%.

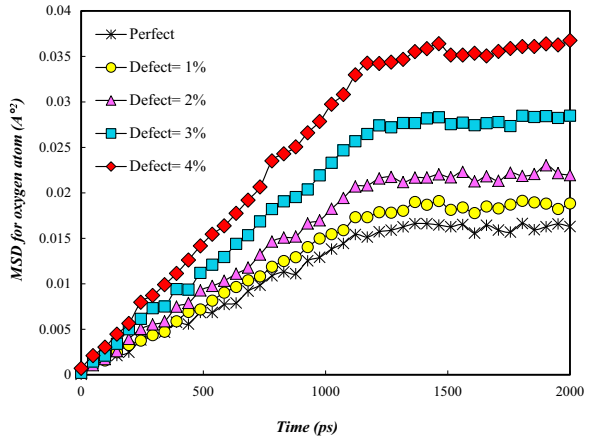

Fig. 6. Oxygen ions mean square displacements versus time in BTO NWs for [001] direction when the vacancy percentage is changed from 0% to 4%.

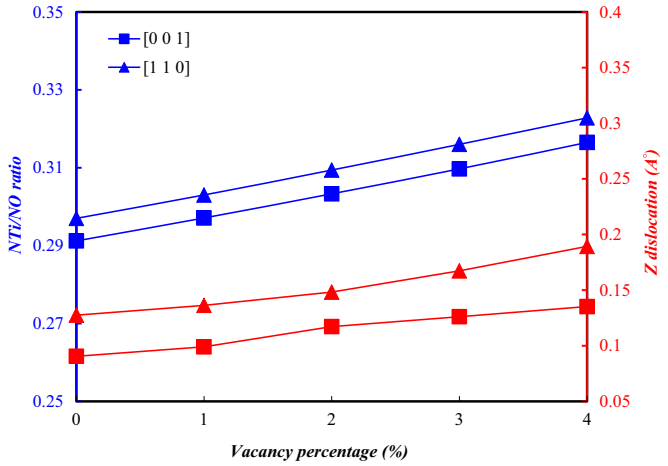

Fig. 7. NTi/NO ratio and z dislocation versus vacancy percentage in BTO NWs for [001] and [110] direction when the vacancy percentage is changed from 0% to 4%.

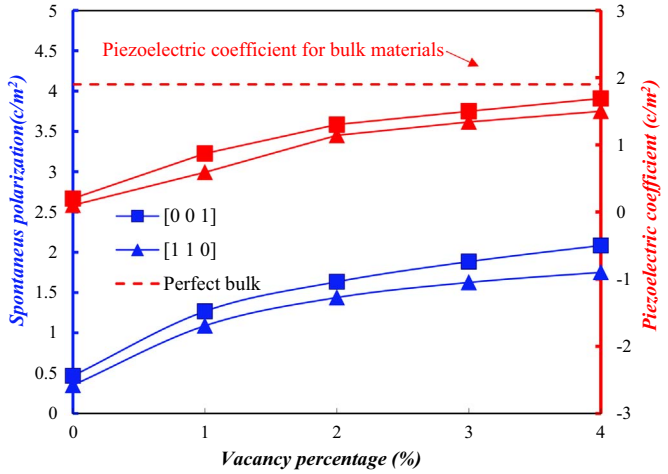

Fig. 8. Plots of spontaneous polarization and piezoelectric coefficient for BTO NWs.

Fig. 7. Dislocations are the average displacement of oxygen atoms in the tension direction. The variation of dislocations with increasing the percentage of vacancy and also the ratio of N_{Ti}/N_O is opposite to that of YS and YG. This observation suggests that the ratio of oxygen atoms may cause that the BTO NWs with axial direction of [110] be softer than axial direction of [001].

Piezoelectric coefficient (d) and spontaneous polarization (SP) of NWs were calculated using Eqs. (5) and (6). The results in terms of vacancy percentage are shown for two orientations of [001] and [110] in Fig. 8.

Results in Fig. 8 show that d and SP increase due to an increase in vacancy percentage. In all of the NWs, for both directions of [001] and [110], the value of d reaches almost to a constant value (bulk) when vacancy increases [52].

The results reported in this figure are comparable with ones reported for YS and YG in Fig. 4. In other words, BTO NWs with higher oxygen vacancy percentage are softer, and have higher atomic displacements as indicated in Fig. 4 and this factor gives rise to higher polarization and piezoelectric coefficients.

It has been proved that oxygen vacancies can have a degrading effect on electromechanical property of piezoelectric materials [53–55]. Many of experimental investigations have indicated that in the polycrystalline perovskite structures such as BTO thin films, the oxygen vacancies accumulates at grain boundaries and twin boundaries [56–58]. This factor causes a pinning effect on domains which degrades the piezoelectric and ferroelectric properties of the system [59–61]. In addition local softening around the grain boundaries (due to accumulation of oxygen vacancies) can lead to an overall reduction in elastic modulus of polycrystalline systems such as thin films [51,62].

It seems that softening mechanism of the oxygen vacancies [51,62], which can result in more mobility of ions and higher value of the polarization and piezoelectric constant, competes with pinning effect. In polycrystalline structures which contain lots of grain boundaries, pinning of domain walls is a dominant factor, but in the individual NWs where there aren't interacting grain boundaries, the softening mechanism overcomes the pinning effect and results in enhancement of polarization and piezoelectric constant. However, an accurate interpretation of piezoelectric enhancement in the oxygen vacancy defected NWs needs a better investigation by using more accurate simulation methods such as Quantum Molecular dynamics methods.

4. Conclusions

The effect of axial direction and oxygen vacancy on electromechanical properties of individual BTO nanowires was investigated by a molecular dynamics simulation method. The results indicate that a 1–4% increase in oxygen vacancy in the BTO NWs, leads to decrease in mechanical constants (e.g., Young's modulus and Yield Stress), while the electrical constants (e.g., piezoelectric coefficient and spontaneous polarization) will increase. It is deduced that in the individual defected BTO NWs the oxygen vacancies with a defined percentage may be the cause of the higher electric field produced with lower applied force. Therefore BTO NWs with oxygen vacancies may be more efficient than the perfect structures for energy harvesting and especially for the nanoscale sensing propose. This result also shows that in NWs [001] and NWs groups [110], the former ([001] direction) can produce a higher electric field and a higher voltage in the same vacancy percentage (maximum of 4%).

References

[1] G.T. Hwang, M. Byun, C.K. Jeong, K.J. Lee, Adv. Healthc. Mater. 4 (2015) 646–658.
[2] B. Kumar, S.-W. Kim, J. Mater. Chem. 21 (2011) 18946–18958.
[3] X. Wang, Nano Energy 1 (2012) 13–24.
[4] K. Yoshii, Y. Yoneda, I. Jarrige, T. Fukuda, Y. Nishihata, C. Suzuki, Y. Ito, T. Terashima, S. Yoshikado, S. Fukushima, J. Phys. Chem. Solids 75 (2014) 339–343.
[5] X. Wang, J. Song, J. Liu, Z.L. Wang, Science 316 (2007) 102–105.
[6] T. Gao, J. Liao, J. Wang, Y. Qiu, Q. Yang, M. Zhang, Y. Zhao, L. Qin, H. Xue, Z. Xiong, J. Mater. Chem. A 3 (2015) 9965–9971.
[7] S. Lee, S.H. Bae, L. Lin, Y. Yang, C. Park, S.W. Kim, S.N. Cha, H. Kim, Y.J. Park, Z.L. Wang, Adv. Funct. Mater. 23 (2013) 2445–2449.
[8] Z. Li, G. Zhu, R. Yang, A.C. Wang, Z.L. Wang, Adv. Mater. 22 (2010) 2534–2537.
[9] R. Yang, Y. Qin, C. Li, G. Zhu, Z.L. Wang, Nano Lett. 9 (2009) 1201–1205.
[10] H.S. Lee, J. Chung, G.T. Hwang, C.K. Jeong, Y. Jung, J.H. Kwak, H. Kang, M. Byun, W.D. Kim, S. Hur, Adv. Funct. Mater. 24 (2014) 6914–6921.

[11] C. Dagdeviren, B.D. Yang, Y. Su, P.L. Tran, P. Joe, E. Anderson, J. Xia, V. Doraiswamy, B. Dehdashti, X. Feng, Proc. Natl. Acad. Sci. USA 111 (2014) 1927–1932.
[12] M. Zhang, T. Gao, J. Wang, J. Liao, Y. Qiu, H. Xue, Z. Shi, Z. Xiong, L. Chen, Nano Energy 11 (2015) 510–517.
[13] S.-H. Shin, Y.-H. Kim, M.H. Lee, J.-Y. Jung, J. Nah, ACS Nano 8 (2014) 2766–2773.
[14] C.K. Jeong, I. Kim, K.-I. Park, M.H. Oh, H. Paik, G.-T. Hwang, K. No, Y.S. Nam, K.J. Lee, Acs Nano 7 (2013) 11016–11025.
[15] A. Koka, Z. Zhou, H.A. Sodano, Energy Environ. Sci. 7 (2014) 288–296.
[16] A.I. Ali, C.W. Ahn, Y.S. Kim, Ceram. Int. 39 (2013) 6623–6629.
[17] S. Devi, A. Jha, Indian J. Phys. 86 (2012) 279–282.
[18] L. Hong, P. Wu, Y. Li, V. Gopalan, C.-B. Eom, D.G. Schlom, L.-Q. Chen, Phys. Rev. B 90 (2014) 174111.
[19] G. Singh, V. Tiwari, P. Gupta, J. Appl. Phys. 107 (2010) 064103.
[20] W. Bucheli, T. Durán, R. Jimenez, Js Sanz, A. Varez, Inorg. Chem. 51 (2012) 5831–5838.
[21] C. Mitra, C. Lin, A.B. Posadas, A.A. Demkov, Phys. Rev. B 90 (2014) 125130.
[22] K.D. Chandrasekhar, S. Mallesh, J.K. Murthy, A. Das, A. Venimadhav, Phys. B: Condens. Matter 448 (2014) 304–311.
[23] H. Jeen, Z. Bi, W.S. Choi, M.F. Chisholm, C.A. Bridges, M.P. Paranthaman, H.N. Lee, Adv. Mater. 25 (2013) 6459–6463.
[24] C.-F. Chen, G. King, R.M. Dickerson, P.A. Papin, S. Gupta, W.R. Kellogg, G. Wu, Nano Energy 13 (2015) 423–432.
[25] D.S. Rivera, T. Ishimoto, M. Koyama, ECS Trans. 57 (2013) 2723–2732.
[26] Y.-K. Choi, T. Hoshina, H. Takeda, T. Teranishi, T. Tsurumi, Appl. Phys. Lett. 97 (2010) 2907.
[27] V.-C. Lo, W.W.-Y. Chung, H. Cao, X. Dai, J. Appl. Phys. 104 (2008) 064105.
[28] C. Voisin, S. Guillemet-Fritsch, P. Dufour, C. Tenailleau, H. Han, J.C. Nino, Int. J. Appl. Ceram. Technol. 10 (2013) E122–E133.
[29] T. Kolodiazhnyi, A. Petric, J. Phys. Chem. Solids 64 (2003) 953–960.
[30] M.G. Shahraki, S. Ghorbanali, H. Savaloni, Solid State Commun. 196 (2014) 40–45.
[31] F. Ercolessi, Spring College in Computational Physics 19, ICTP, Trieste, 1997.
[32] D.C. Rapaport, in, Cambridge University Press, Cambridge, 1996.
[33] D. Khatib, R. Migoni, G. Kugel, L. Godefroy, J. Phys.: Condens. Matter 1 (1989) 9811.
[34] S. Tinte, M. Stachiotti, M. Sepliarsky, R. Migoni, C. Rodriguez, J. Phys.: Condens. Matter 11 (1999) 9679.
[35] H. Rafii-Tabar, Phys. Rep. 390 (2004) 235–452.
[36] E. Heifets, S. Dorfman, D. Fuks, E. Kotomin, Thin Solid Films 296 (1997) 76–78.
[37] G. Lewis, C. Catlow, J. Phys. C: Solid State Phys. 18 (1985) 1149.
[38] Y. Zulueta, J. Dawson, Y. Leyet, F. Guerrero, J. Anglada-Rivera, M. Nguyen, Phys. Status Solidi (b) 253 (2016) 345–350.
[39] M. Zhou, Proc. R. Soc. Lond. Ser. A: Math., Phys. Eng. Sci. 459 (2003) 2347–2392.
[40] C. Meis, J.L. Fleche, Solid State Ion. 101 (1997) 333–335.
[41] S. Plimpton, A. Thompson, P. Crozier, in, 2012.
[42] L. Verlet, Phys. Rev. 159 (1967) 98.
[43] W.-J. Chang, Microelectron. Eng. 65 (2003) 239–246.
[44] D. Roylance, Massachusetts Institute of Technology study, Cambridge, 2001.
[45] K.L. Duncan, Y. Wang, S.R. Bishop, F. Ebrahimi, E.D. Wachsman, J. Am. Ceram. Soc. 89 (2006) 3162–3166.
[46] Y. Wang, K. Duncan, E.D. Wachsman, F. Ebrahimi, Solid State Ion. 178 (2007) 53–58.
[47] S.S. Bhat, U.V. Waghmare, U. Ramamurty, Comput. Mater. Sci. 99 (2015) 133–137.
[48] Z. Li, S.K. Chan, M. Grimsditch, E. Zouboulis, J. Appl. Phys. 70 (1991) 7327–7332.
[49] J. Freire, R. Katiyar, Phys. Rev. B 37 (1988) 2074.
[50] M. Lucas, Z.L. Wang, E. Riedo, Appl. Phys. Lett. 95 (2009) 051904.
[51] A.N.A.B. Berry, Academic Press, New York, 1972, 677 28 73, 1973.
[52] A. Schaefer, H. Schmitt, A. Dorr, Ferroelectrics 69 (1986) 253–266.
[53] C.-P. De Araujo, J. Cuchiaro, L. McMillan, M. Scott, J. Scott, Nature 374 (1995) 627–629.
[54] Y. Wang, K. Wang, C. Zhu, T. Wei, J. Zhu, J.-M. Liu, J. Appl. Phys. 101 (2007) 6104.
[55] J. Scott, M. Dawber, Appl. Phys. Lett. 76 (2000) 3801–3803.
[56] T. Oyama, N. Wada, H. Takagi, M. Yoshiya, Phys. Rev. B 82 (2010) 134107.
[57] M. Calleja, M.T. Dove, E.K. Salje, J. Phys.: Condens. Matter 15 (2003) 2301.
[58] B. Liu, V.R. Cooper, Y. Zhang, W.J. Weber, Acta Mater. 90 (2015) 394–399.
[59] B. Cheng, M. Gabbay, G. Fantozzi, Defect and Diffusion Forum, Trans Tech Publ, 2002, pp. 143–146.
[60] L. He, D. Vanderbilt, Phys. Rev. B 68 (2003) 134103.
[61] W. Li, A. Chen, X. Lu, J. Zhu, J. Appl. Phys. 98 (2005) 024109.
[62] D. Shilo, H. Drezner, A. Dorogoy, Phys. Rev. Lett. 100 (2008) 035505.